Pergamon

PII: S0301-9322(96)00036-5

Int. J. Multiphase Flow Vol. 22, No. 6, pp. 1123–1142, 1996

0301-9322/96 $15.00 + 0.00

DISCHARGE FROM A SMOOTH STRATIFIED TWO-PHASE REGION THROUGH TWO HORIZONTAL SIDE BRANCHES LOCATED IN THE SAME VERTICAL PLANE

I. G. HASSAN[1], H. M. SOLIMAN[1], G. E. SIMS[1] and J. E. KOWALSKI[2]

[1]Department of Mechanical and Industrial Engineering, University of Manitoba, Winnipeg, Manitoba, Canada R3T 5V6

[2]Thermalhydraulics Branch, AECL Research, Pinawa, Manitoba, Canada R0E 1L0

(Received 3 July 1995; in revised form 4 December 1995)

Abstract—Experimental data are presented for the mass flow rate and quality of two-phase (air–water) discharge from a stratified region through two side branches (6.35 mm i.d.) with their parallel centrelines located in a vertical plane. These data correspond to different values of the interface level between the onset of gas entrainment at the upper branch to the onset of liquid entrainment at the lower branch for test-section pressures of 316 and 517 kPa, test-section-to-separators pressure difference ranging from 40 to 235 kPa, branch separating distance to diameter ratio ranging from 1.5 to 8 and different hydraulic resistances of the lines connecting the test section to the separators. Normalized plots are shown to be capable of absorbing the effects of some independent variables within the tested range of operating conditions. Empirical relations were developed for the prediction of the two-phase mass flow rate and quality in terms of normalized parameters. These relations represent the data with a high degree of correlation. Copyright © 1996 Elsevier Science Ltd.

Key Words: dual discharge, small breaks, two-phase flow, experimental data, empirical correlation

1. INTRODUCTION

Several industrial applications involve two-phase flow discharging from a stratified region through single or multiple branches. Examples of these applications include: the flow through small breaks in horizontal cooling channels of nuclear reactors during postulated loss-of-coolant accidents; the flow distribution in CANDU header–feeder systems (multiple branches) during accident scenarios; and two-phase distribution systems in general, where a certain incoming stream fed into a large header or chamber is divided among a number of discharging streams, for instance in a shell-and-tube heat exchanger. Knowledge of the flow phenomena involved, as well as the mass flow rate and quality of all discharging streams is obviously essential for the design and/or performance prediction of such systems.

For the case of a single discharge from a large flow channel under stratified flow conditions, Zuber (1980) pointed out that the phenomena of gas and liquid entrainment will influence the flow through the branch. He proposed simplified correlations for the onsets of these phenomena in terms of relevant system parameters and branch orientation (top, bottom or side). Later, detailed experiments were reported on the onsets of gas and liquid entrainment, two-phase mass flux and quality during discharge from a large stratified region (with or without main flow) through a single branch with different orientations (e.g. Smoglie & Reimann 1986; Schrock *et al.* 1986; Yonomoto & Tasaka 1988, 1991; Micaelli & Mempontiel 1989; Hassan *et al.* 1994).

In situations where multiple discharge takes place simultaneously from several branches, the existing single-branch correlations may not apply. Initial steps towards understanding these systems were undertaken by Parrott *et al.* (1991) and Armstrong *et al.* (1992) who investigated the onsets of gas and liquid entrainment, respectively, during discharge from stratified two-phase regions through two side branches. However, no information is available yet in the open literature for the evaluation of the two-phase mass flow rate and quality during dual discharge.

The objective of the present investigation is to conduct a basic experiment in order to measure the two-phase discharge from a large stratified region through two side branches of the same diameter d, separated by a vertical distance L centre-to-centre. This experiment is obviously a first step towards understanding situations of multiple discharge from two-phase headers. The main questions to be answered are: "What is the influence of discharge from one branch on the discharge from the other branch?", "How do these two discharges differ from the case of a single discharge?", and "What is the influence of the separating distance L?"

2. EXPERIMENTAL INVESTIGATION

2.1. Experimental parameters

Figure 1 shows the geometrical and flow parameters relevant to this experiment. Two branches of equal diameter d and a vertical separating distance L (centre-to-centre) are placed on the side of a large reservoir containing stratified layers of air and water at a pressure P_0. The two discharging streams are directed (via individual connecting lines) to their respective separators maintained at the same pressure P_S. Thus, the experiment is conducted under the condition that the pressure drop, $\Delta P = P_0 - P_S$, is the same for both connecting lines. As well, the connecting lines were designed to have the same hydraulic resistance, R, as defined later. Equal values of R imply equal single-phase mass flow rates through the connecting lines for equal ΔP. Under these conditions, the mass flow rate and quality of both discharging streams are expected to depend on P_0, ΔP, R, L/d, and the location of the air–water interface relative to the branches.

For fixed values of P_0, ΔP, R and L/d, let us consider the dependence of the flow from both branches on the location of the interface. A detailed description of the flow phenomena, including interface shapes, is given in the appendix. At high interface levels above the upper branch, the discharge from both branches will be in the form of single-phase liquid with essentially equal mass flow rates, $\dot{m}_{L,A} = \dot{m}_{L,B}$, where $\dot{m}_{L,A}$ is the liquid mass flow rate at the upper branch and $\dot{m}_{L,B}$ is the liquid mass flow rate at the lower branch. Lowering the interface level, a critical height is reached where the onset or beginning of gas entrainment occurs at the upper branch with $h_A = h_{BGE,A}$ and $\dot{m}_{L,A} = \dot{m}_{L,BGE,A}$, where h_A is the vertical distance between the flat interface and the centreline of the upper branch (positive in the upward direction), $h_{BGE,A}$ is the magnitude of h_A at the onset of gas entrainment at the upper branch and $\dot{m}_{L,BGE,A}$ is the magnitude of $\dot{m}_{L,A}$ at the onset of gas entrainment at the upper branch. For $h_A \geqslant h_{BGE,A}$, the three quantities $\dot{m}_{L,A}$, $\dot{m}_{L,B}$ and $\dot{m}_{L,BGE,A}$ are essentially equal. The hydraulic resistance for both connecting lines is defined as

$$R = \sqrt{\Delta P}/\dot{m}_{L,BGE}. \qquad [1]$$

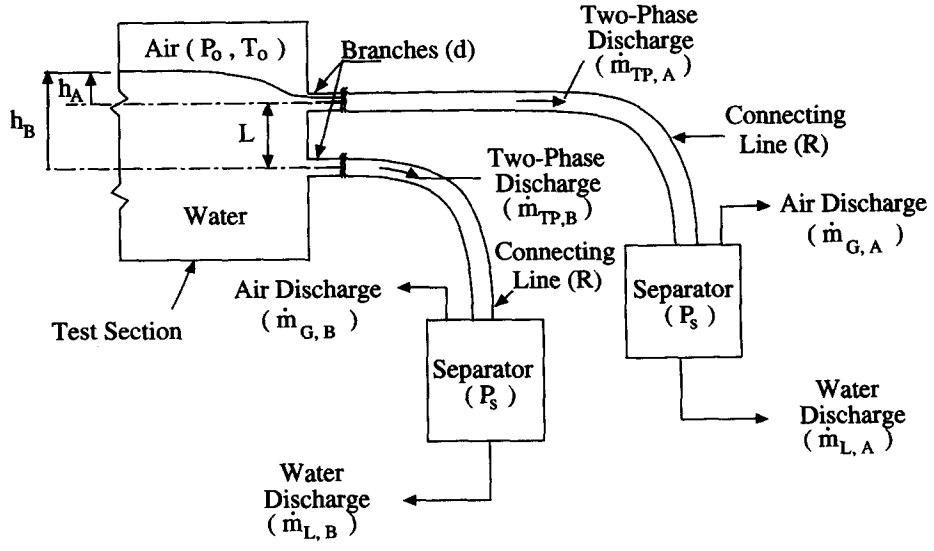

Figure 1. Relevant experimental parameters.

A further lowering of the interface results in a two-phase discharge at the upper branch with a mass flow rate $\dot{m}_{TP,A}$, while the single-phase liquid flow at the lower branch remains essentially unchanged. The two-phase flow from the upper branch is split in its separator into liquid ($\dot{m}_{L,A}$) and gas ($\dot{m}_{G,A}$) components, whereby

$$\dot{m}_{TP,A} = \dot{m}_{L,A} + \dot{m}_{G,A} \quad [2]$$

and the quality at the upper branch is given by

$$x_A = \dot{m}_{G,A}/\dot{m}_{TP,A}. \quad [3]$$

As h_A decreases, $\dot{m}_{TP,A}$ decreases while x_A increases.

Two other critical heights are next reached with further lowering of the interface: (i) the "onset" of liquid entrainment at the upper branch corresponding to $h_A = h_{BLE,A}$, $x_A = 1$ and $\dot{m}_{G,A} = \dot{m}_{G,BLE,A}$, where $h_{BLE,A}$ is the magnitude of h_A at the onset of liquid entrainment at the upper branch and $\dot{m}_{G,BLE,A}$ is the gas mass flow rate at the upper branch corresponding to the onset of liquid entrainment at that branch (although on lowering the interface level, at this point the flow changes from there being liquid entrained in the branch to there being no liquid entrained in the branch, the term "onset" or "beginning" is used, rather than "end", in keeping with the existing literature); and (ii) the onset of gas entrainment at the lower branch with $h_B = h_{BGE,B}$ and $\dot{m}_{L,B} = \dot{m}_{L,BGE,B} = \dot{m}_{L,BGE,A}$, where h_B is the vertical distance between the flat interface and the centreline of the lower branch (positive in the upward direction), $h_{BGE,B}$ is the magnitude of h_B at the onset of gas entrainment at the lower branch and $\dot{m}_{L,BGE,B}$ is the magnitude of $\dot{m}_{L,B}$ at the onset of gas entrainment at the lower branch. The order in which these two critical conditions are encountered as the interface is lowered depends on the values of ΔP, R and L/d. For large values of L/d and/or small values of ΔP and/or large values of R, the onset of liquid entrainment at the upper branch precedes the onset of gas entrainment at the lower branch as the interface is lowered. For such conditions, the two branches are expected to behave as two independent single branches with limited (if any) interaction between them. On the other hand, for conditions of small L/d and/or large ΔP and/or small R, the onset of liquid entrainment at the upper branch is encountered at a lower interface level than that for the onset of gas entrainment at the lower branch. The branches will then have mutual interaction and the flow (magnitude and quality) from both branches is expected to deviate from the single-branch case.

Finally, the onset of liquid entrainment at the lower branch is encountered at a lower interface level with $h_B = h_{BLE,B}$, $x_B = 1$ and $\dot{m}_{G,B} = \dot{m}_{G,BLE,B}$, where $h_{BLE,B}$ is the magnitude of h_B at the onset of liquid entrainment at the lower branch, x_B is the quality at the lower branch, $\dot{m}_{G,B}$ is the gas mass flow rate at the lower branch and $\dot{m}_{G,BLE,B}$ is the magnitude of $\dot{m}_{G,B}$ at the onset of liquid entrainment at the lower branch. For $h_B \leqslant h_{BLE,B}$, the discharge from both branches will be in the form of single-phase gas flow with flow rates $\dot{m}_{G,A} = \dot{m}_{G,B} = \dot{m}_{G,BLE,A} = \dot{m}_{G,BLE,B}$.

The focus in this study will be on the two-phase region corresponding to $h_{BLE} \leqslant h \leqslant h_{BGE}$ for both branches in order to investigate the behavior of $\dot{m}_{TP}$ and x within this region. The experimental data will be sought in a systematic fashion so that the influence of each independent parameter can be assessed individually.

2.2. Experimental test facility

The flow loop is shown schematically in figure 2. An immersion-type circulating pump was used to supply distilled water to the test section at a rate adjusted by a by-pass line. The temperature of the water was held steady (near room temperature) by a cooling coil. The test section was connected to an air supply equipped with a feed-back pressure controller which maintained the test-section pressure, P_0, steady at a preset value.

The test section is basically a large reservoir manufactured from type 304 stainless-steel sections, except for a clear acrylic pipe section near the outlet flange for visual observation of the flow phenomena. The construction details of the test section were reported by Parrott *et al.* (1991). The first part of any branch was a hole, 6.35 mm in diameter and 127 mm long, machined in a brass block and bolted to the stainless-steel outlet flange. Thus, each branch had a straight length of 20 diameters before any bends or area changes were incorporated; downstream of this, the components in each line were the same so that the geometries of the two branches from the reservoir

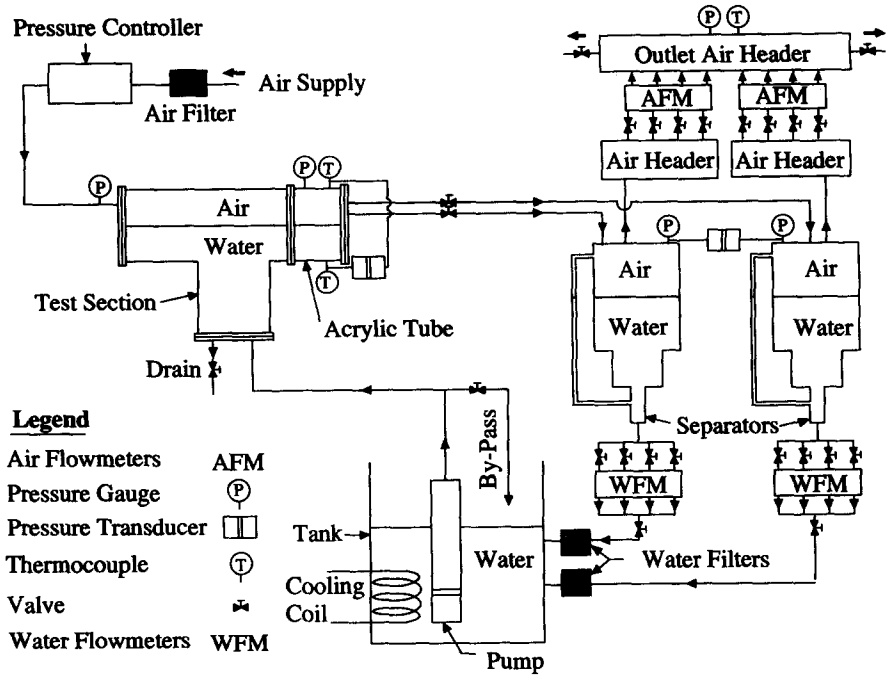

Figure 2. Schematic diagram of the experimental test facility.

to the separators were the same. Different brass blocks were machined to provide $L/d = 1.5$, 2, 3 and 8. A surveying transit was used to ensure that the faces of the flange and the block were vertical and that the centrelines of the branches fell on a straight vertical line. Two pressure taps, one on the air side and the other on the water side, were installed on the outlet flange and connected to a differential pressure transducer in order to measure the liquid height in the test section.

The two-phase flows leaving the test section through the two branches were directed to their respective separators where the air and water were split by centrifugal action. A pressure tap was installed on the air side of each separator and connected to a differential pressure transducer. The reading of this transducer was monitored continuously and adjustments to outlet flow rates were made (if necessary) in order to ensure that the pressure difference between the two separators was at or near zero. The flow rates of air and water leaving each separator were measured by a bank of four variable-area-type flow meters with overlapping ranges. Each of these flow-measuring stations covered the range of 15 cm^3/min–0.0415 m^3/min on the water side and 198 cm^3/min–1.3 m^3/min at standard conditions on the air side.

The temperature and pressure within the test section and separators, as well as other locations within the loop were recorded during the experiment. All flow meters, thermocouples, and pressure gauges were calibrated before testing began.

2.3. *Experimental procedure*

A total of 32 data sets were collected in this investigation, each corresponding to a certain combination of P_0, ΔP, R and L/d. Each data set contains 20–30 different locations of the interface between $h_{BGE,A}$ and $h_{BLE,B}$ with measurements of the flow rate from each branch performed at each interfacial location.

Before starting the experiments with a new value of L/d, the hydraulic resistances of the two connecting lines were set essentially equal. Generally the control of R in terms of a major change (e.g. 3000 to 1670 to 1000 $(kg \cdot m)^{-1/2}$) was by the insertion of a cylindrical plug with a central hole, the diameter of which depended on the desired R. The plugs in each line were nominally of the same internal diameter; however, to achieve single-phase liquid flow rates in each branch with the required tolerance (within 3% of each other), the internal diameter of one of the two plugs was slightly enlarged. The corresponding deviations in the single-phase gas flow rates from the two

branches were 3% or less for 29 of the data sets and 4.3% for the remaining three sets. After adjusting R for a given L/d, appropriate values of P_0 and ΔP were fixed and the following procedure was followed in collecting the data for the set:

(1) The conditions at the onset of gas entrainment at the upper branch ($h_{BGE,A}$ and $\dot{m}_{L,BGE,A}$) were established first. The air–water interface location (height) was set at a high value and was reduced in small steps, at which the liquid flow rate was measured under steady conditions. As the onset was approached, the liquid level was slowly lowered further until gas was suddenly entrained at the branch; this onset was observed visually through the transparent part of the test section. The steady-state flow rate just before the onset gave $\dot{m}_{L,BGE,A}$ and the reading of the pressure transducer immediately following the onset gave $h_{BGE,A}$.
(2) Knowing that the magnitudes of $h_{BGE,A}$ and $h_{BLE,B}$ are roughly equal, the vertical distance between these two locations was divided into a number (in the range of 20–30) of equal intervals. The experiment was then conducted at decreasing values of h. At each h, the liquid level was held constant for a sufficient period of time that allowed the flow into each separator to be measured accurately.
(3) Three other onsets were encountered with decreasing h; these were the onsets of liquid entrainment at the upper branch, and gas and liquid entrainment at the lower branch. All these onsets were detected visually. As each one of these onsets was approached, the liquid level was lowered in fine increments so that the corresponding h and $\dot{m}$ were accurately determined. With the water level just slightly above that for the condition of the onset of liquid entrainment at either branch, a stream of water was seen to be pulled up from the interface through the branch. Decreasing the level caused this stream to become thinner until it suddenly disappeared at the "onset".

2.4. *Experimental uncertainty*

An estimate of the uncertainties in the independent and dependent variables was made in the fashion described by Moffat (1988) and Kline & McClintock (1953). All uncertainties quoted here are at "odds" of 20 to 1. The uncertainties are meant to accommodate: the accuracy of the calibrating device, the error in fitting an equation (for computer data reduction) to the calibration data, discrimination uncertainties in the measuring instruments and unsteadiness in the process. Pressure gauges were calibrated using a deadweight tester, thermocouples using a standard mercury-in-glass thermometer, gas rotameters using wet test meters and venturi meters (in turn the calibrations of which were traceable to NIST standards) and liquid rotameters using a weigh-and-time method. The pressure transmitter used for measuring h was calibrated against a micromanometer and the digital voltmeter used in the calibration was subsequently used in the normal running of the experiments; for both calibration and subsequent experiments the sensitivity was approximately 35 mV per mm of water; the discrimination on the digital voltmeter was ± 1 mV.

The results of the uncertainty analysis follow. The uncertainty in P_0 (absolute pressure) was $\pm 0.9\%$; the uncertainty in ΔP for data set nos. 3, 13, 23 and 29 ($\Delta P = 40$ kPa, the smallest ΔP) was approximately $\pm 7.9\%$, while for the other data sets (higher ΔP) it was $\pm 3.9\%$ or less. The maximum uncertainty in the flow rates $\dot{m}_G$, $\dot{m}_L$ and $\dot{m}_{TP}$ was ± 4.0, 2.5 and 4.7%, respectively. The uncertainty in temperature measurement was ± 0.25°C. The maximum uncertainty in the quality x was $\pm 4.7\%$. The maximum uncertainty in R was $\pm 4.7\%$. The absolute uncertainty in h was ± 0.14 mm; for the cases where there was interaction between the two branches (combinations of small L/d and/or large ΔP and/or small R), because of unsteadiness of the interface there was more uncertainty in determining $h_{BLE,A}$ and $h_{BGE,B}$ (both ± 0.38 mm) than in $h_{BLE,B}$ and $h_{BGE,A}$ (both ± 0.23 mm); for the case of no interaction between the two branches, the uncertainty in the four onsets was the same (± 0.23 mm). The uncertainty in h amounted to approximately $\pm 0.7\%$ of $(h_{BGE} - h_{BLE})$.

For the dimensionless quantity H (defined later and having a range of 0–1), the uncertainty δH was a maximum of ± 0.02. At the upper branch and in the range $0.2 \leqslant H \leqslant 1$, $\delta H/H$ decreased from a value of $\pm 8\%$ or less at $H = 0.2$ to $\pm 1.5\%$ at $H = 1$; the uncertainty in $\delta H/H$ increased with decreasing H and at the smallest finite H ($=0.1$) was $\pm 13.5\%$ or less. At the lower branch

and in the range $0.2 \leqslant H \leqslant 1$, $\delta H/H$ decreased from a value of $\pm 5.5\%$ or less at $H = 0.2$ to $\pm 2.0\%$ or less at $H = 1$; at $H = 0.1$, $\delta H/H$ was $\pm 13\%$ or less, and increased to larger values as H decreased further.

For the dimensionless quantity M (defined later and having a range of 0–1), δM varied between ± 0.003 and ± 0.038, smaller values being associated with small M and larger values being associated with large M. At the upper branch (the numbers which follow in brackets are for the lower branch) and in the range $0.1 \leqslant M \leqslant 1$, the maximum uncertainty in $\delta M/M$ was $\pm 5.5\%$ ($\pm 5\%$); the uncertainty in $\delta M/M$ increased with decreasing M, was $\pm 10\%$ or less ($\pm 8\%$ or less) at $M = 0.05$ and increased to large values as M approached zero.

3. RESULTS AND DISCUSSION

The operating conditions for the 32 data sets generated in this investigation are listed in table 1. For $L/d = 1.5$, set nos 1–3 and set nos 6–8 explore the effect of ΔP at fixed P_0 and R. The influence of R at fixed P_0 and ΔP can be examined from set nos 1, 4 and 5, or set nos 6, 9 and 10. A similar test matrix was followed for $L/d = 2$. However, for $L/d = 3$ and 8, it was decided not to include the influence of R at fixed P_0 and ΔP because sufficient information on this effect had been gained from the results of $L/d = 1.5$ and 2. Values of P_0, ΔP and R used in this investigation are practically identical to those used by Hassan *et al.* (1994) for the case of single-branch discharge; therefore, influences of the discharge at the second branch can be clearly isolated.

In order to determine whether choking conditions occurred in the present experiments, the data for $\dot{m}_{TP}$ for the single-discharge case (Hassan *et al.*, 1994), using the same combinations of P_0, ΔP and R as reported here, were compared with predicted critical flow rates as obtained from two

Table 1. Nominal operating conditions

Set No.	L/d	P_0 (kPa)	ΔP (kPa)	R $(\text{kg}\cdot\text{m})^{-1,2}$
1	1.5	316	123	1000
2			82	
3			40	
4			123	1670
5				3000
6		517	235	1000
7			166	
8			97	
9			236	1670
10				3000
11	2.0	316	123	1000
12			82	
13			40	
14			123	1670
15				3000
16		517	235	1000
17			166	
18			97	
19			236	1670
20				3000
21	3.0	316	123	1000
22			82	
23			40	
24		517	235	
25			166	
26			97	
27	8.0	316	123	1000
28			82	
29			40	
30		517	235	
31			166	
32			97	

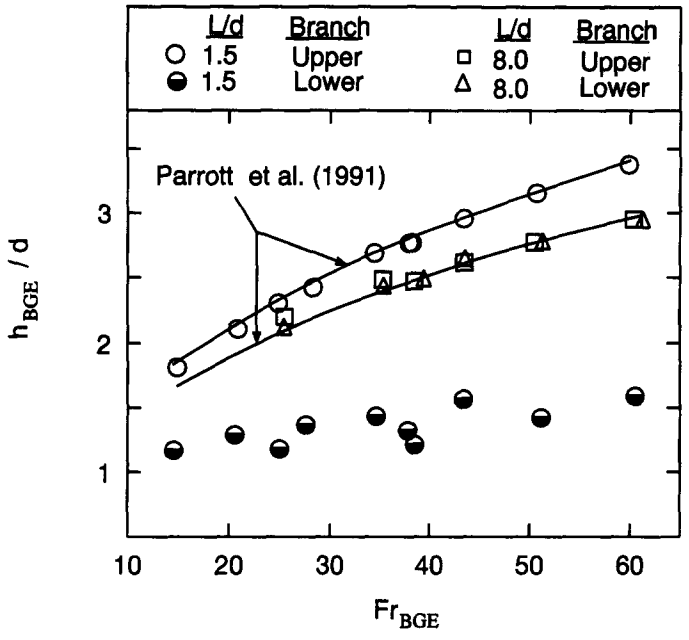

Figure 3. The onset of gas entrainment.

models. The models were the "homogeneous frozen flow model" (Whalley 1987) and that by Henry & Fauske (1971). For fixed P_0, ΔP and R, the value at a given x, of the ratio of the actual $\dot{m}_{TP}$ to the predicted critical mass flow rate at any x never exceeded 0.8. An experimental check was conducted for the limiting case of single-phase air flow by increasing ΔP beyond the maximum value otherwise used in the experiments and no choking occurred. It is reasonable to conclude that choking did not occur with the single-discharge case, and we extend this conclusion to the dual-discharge case.

3.1. *Onsets of gas and liquid entrainment*

The critical heights at the onsets of gas and liquid entrainment were measured for both branches in each of the 32 data sets. A sample of these results is shown in figure 3 (gas entrainment) and figure 4 (liquid entrainment). Data for $L/d = 1.5$ and 8 are shown in both figures; the trend for intermediate values of L/d is monotonic. The predicted values of $h_{BGE,A}$ from the empirical correlation of Parrott *et al.* (1991) are shown in figure 3 and the predicted values of $h_{BLE,B}$ from the theoretical analysis of Armstrong *et al.* (1992) are shown in figure 4. The results in figures 3 and 4 are presented in terms of Froude number at the onset of gas entrainment, Fr_{BGE}, and Froude number at the onset of liquid entrainment, Fr_{BLE}, respectively. These dimensionless groups are defined by

$$Fr_{BGE} = (4/\pi)\dot{m}_{L,BGE}/\sqrt{gd^5\rho_L(\rho_L - \rho_G)} \quad [4]$$

and

$$Fr_{BLE} = (4/\pi)\dot{m}_{G,BLE}/\sqrt{gd^5\rho_G(\rho_L - \rho_G)}, \quad [5]$$

where g, ρ_L and ρ_G are the gravitational acceleration, the liquid density and the gas density, respectively.

Figure 3 shows that $h_{BGE,A}$ and $h_{BGE,B}$ are nearly identical for $L/d = 8$, which suggests very little interaction between the branches at this separating distance. The interaction between the branches intensifies as L/d decreases and as a consequence, $h_{BGE,A}$ increases while $h_{BGE,B}$ decreases. This trend is consistent with the observation that just before the onset of gas entrainment at the upper branch, both branches are fully submerged in liquid and the lower branch would thus assist the upper branch in entraining gas from higher interface locations, while on the other hand, just before the onset of gas entrainment at the lower branch, only the lower branch is fully submerged in liquid

and thus the upper branch competes with (rather than assists) the lower branch for gas flow. The deviation between $h_{BGE,A}$ and $h_{BGE,B}$ increases monotonically up to the values shown in figure 3 for $L/d = 1.5$. The correlation of Parrott *et al.* (1991) is in excellent agreement with the present data of $h_{BGE,A}$ for $L/d = 1.5$ and 8.

Figure 4 also shows that the interaction between the branches is small at $L/d = 8$ with nearly identical values of $h_{BLE,A}$ and $h_{BLE,B}$. The deviation between these two critical heights increases continuously as L/d decreases. The trend in this case is for $|h_{BLE,A}|$ to decrease and $|h_{BLE,B}|$ to increase as L/d decreases. This trend is consistent with the observation that just after the onset of liquid entrainment at the lower branch, both branches are receiving pure gas flow and the upper branch would thus assist the lower branch in entraining liquid from lower interface locations. On the other hand, just after the onset of liquid entrainment at the upper branch, only the upper branch is receiving pure gas flow and thus the lower branch competes with the upper branch for liquid flow. The theoretical predictions of Armstrong *et al.* (1992) are in good agreement with the present data of $h_{BLE,B}$ for $L/d = 1.5$ and 8.

Empirical correlations were developed for the critical heights at all four onsets based on the present data. These correlations, obtained by least-square fitting, are given by the following relations:

$$h_{BGE,A}/d = 0.57[A_1 \mathrm{Fr}_{BGE}]^{0.4}, \quad [6]$$

$$h_{BGE,B}/d = 0.57\mathrm{Fr}_{BGE}^{A_2}, \quad [7]$$

$$|h_{BLE,A}|/d = 0.87\mathrm{Fr}_{BLE}^{A_3}, \quad [8]$$

and

$$|h_{BLE,B}|/d = 0.87[A_4 \mathrm{Fr}_{BLE}]^{0.31}, \quad [9]$$

where,

$$A_1 = 1 + \exp[-1.96(L/d)^{1.2}/\mathrm{Fr}_{BGE}^{0.32}], \quad [10]$$

$$A_2 = 0.4 - 0.223\exp[-0.415(L/d)^{1.5}/\mathrm{Fr}_{BGE}^{0.20}], \quad [11]$$

$$A_3 = 0.31 - 0.13\exp[-0.209(L/d)^{1.5}/\mathrm{Fr}_{BLE}^{0.20}] \quad [12]$$

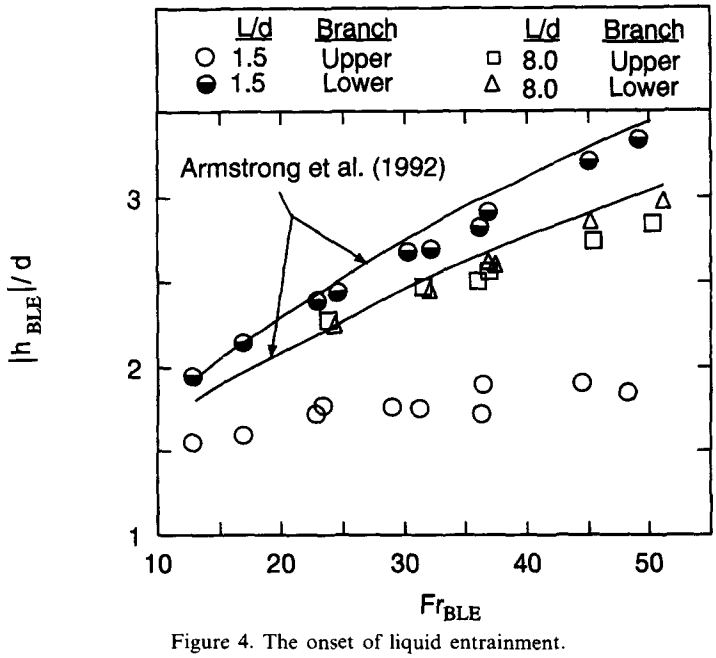

Figure 4. The onset of liquid entrainment.

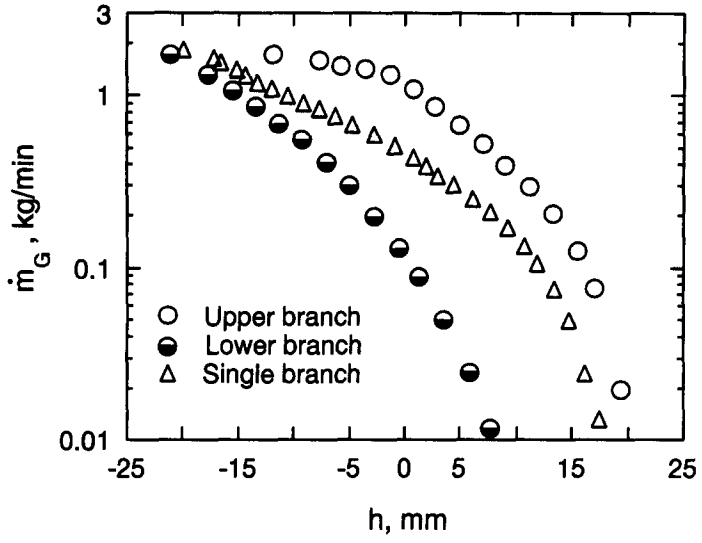

Figure 5. Gas mass flow rate for data set no. 6.

and

$$A_4 = 1 + \exp[-2.27(L/d)^{1.2}/\mathrm{Fr}_{\mathrm{BLE}}^{0.32}]. \quad [13]$$

The above relations converge to the correct limits at the two extremes of L/d. For $L/d = \infty$, we get $A_1 = A_4 = 1$, $A_2 = 0.4$ and $A_3 = 0.31$, and [6]–[9] converge to the single-branch relations reported by Hassan (1995). For $L/d = 0$, we get $A_1 = A_4 = 2$, and [6] and [9] reduce to the single-branch relations with twice the values of Froude number; i.e. a single branch with twice the suction.

The predictive relations given by [6]–[13] are in excellent agreement with the present data. The root-mean-square values of the deviation between the present data and [6]–[9] are 1.9, 4.4, 3.8 and 2.9%, respectively.

3.2. *Mass flow rate and quality*

In order to explain the trends from the current results, the presentation is made first in terms of dimensional quantities. Measured values of $\dot{m}_G$, $\dot{m}_L$, $\dot{m}_{TP}$ and x for data set no. 6 are presented in figures 5–8, respectively. For the dual-discharge case, the h of the abscissa on these figures is

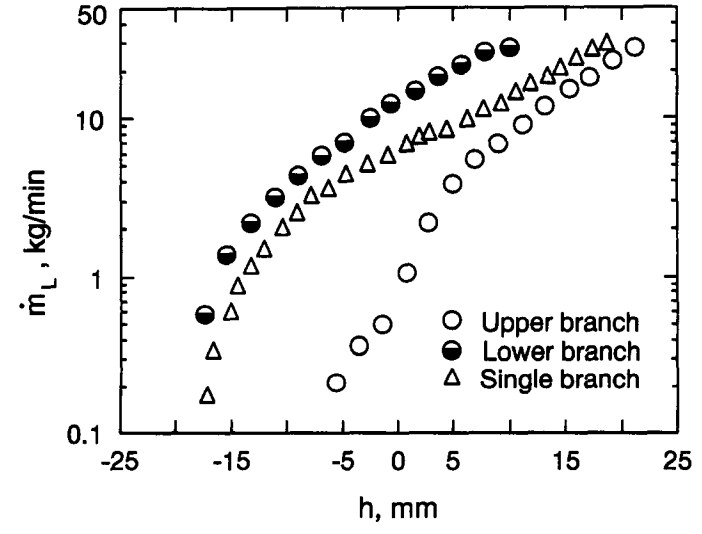

Figure 6. Liquid mass flow rate for data set no. 6.

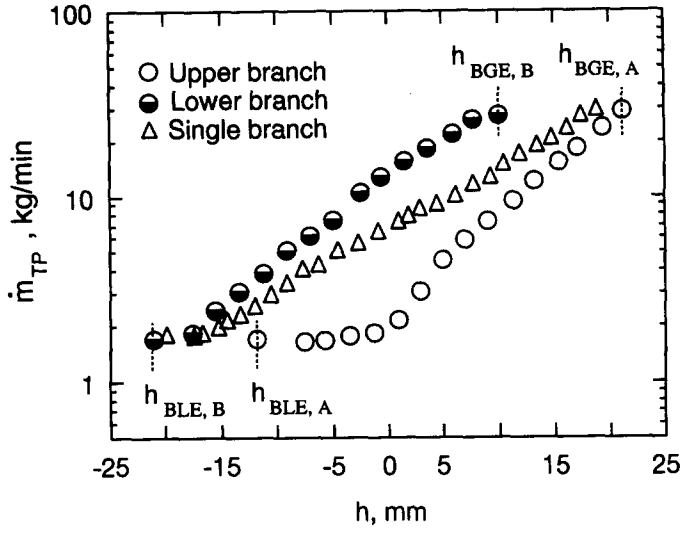

Figure 7. Two-phase mass flow rate for data set no. 6.

h_A for the upper branch and h_B for the lower branch. This data set corresponds to the highest P_0 and ΔP and lowest R, a combination that results in the highest gas and liquid flow rates. In addition, this set corresponds to the smallest L/d; therefore, the effects due to dual discharge seen in figures 5–8 are the most pronounced in this study. Results from Hassan *et al.* (1994) for single discharge at the same P_0, ΔP and R are shown for comparison. Figure 5 shows an increase in air flow rate at the upper branch and a decrease at the lower branch relative to the single-branch case. Figure 6 shows that $\dot{m}_L$ follows an opposite trend to that of $\dot{m}_G$. These opposite trends are in fact consistent and can be explained by observing that all the data in figures 5 and 6 correspond to the same ΔP and thus, an increase in $\dot{m}_G$ at one branch would require a decrease in $\dot{m}_L$ at the same branch. The results in figures 7 and 8 follow easily from those in figures 5 and 6. It is clear from figures 5–8 that the results for dual discharge cannot be predicted from those of single discharge and thus the need for the present data is justified.

The trends shown in figures 5–8 for data set no. 6 are typical of all data sets. The magnitude of the deviation between the results at the upper and lower branches was found to decrease with an increase in L/d or R, or a decrease in ΔP. For data set nos 27–32 corresponding to $L/d = 8$,

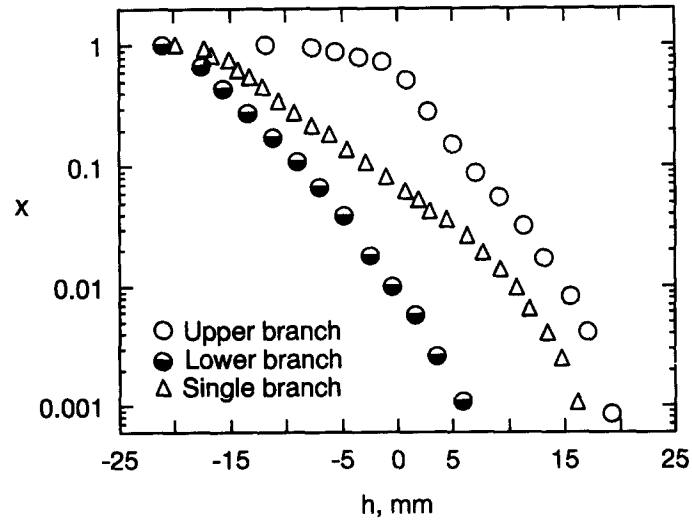

Figure 8. Discharge quality for data set no. 6.

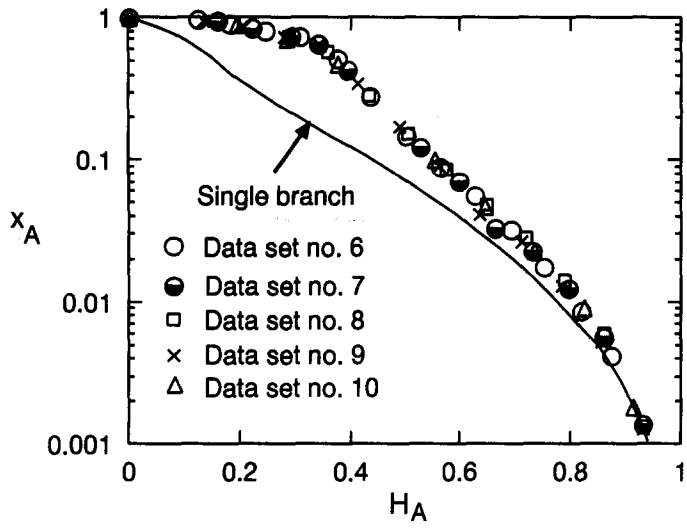

Figure 9. Values of x_A for data set nos 6–10.

insignificant differences between upper, lower and single branch results were obtained for all values of P_0, ΔP and R tested in this study.

An attempt was made to plot the data in a normalized fashion so that the influences of some independent variables may be absorbed. This was done using the following definitions (first introduced by Hassan *et al.*, 1994) for the normalized liquid level and the normalized mass flow rate, respectively:

$$H_i = (h_i - h_{\mathrm{BLE},i})/(h_{\mathrm{BGE},i} - h_{\mathrm{BLE},i}), \quad i = A \text{ or } B \qquad [14]$$

and

$$M_i = (\dot{m}_{\mathrm{TP},i} - \dot{m}_{\mathrm{G,BLE},i})/(\dot{m}_{\mathrm{L,BGE},i} - \dot{m}_{\mathrm{G,BLE},i}), \quad i = A \text{ or } B. \qquad [15]$$

The discharge quality at the upper branch for set nos 6–10 is shown in figure 9 and the normalized two-phase flow rate from the lower branch for set nos 1–5 is shown in figure 10. These results show that the influences of ΔP and R can be absorbed (within the tested range) by plotting x vs H and M vs H. However, the collapsed data in both figures deviate from the single-branch results.

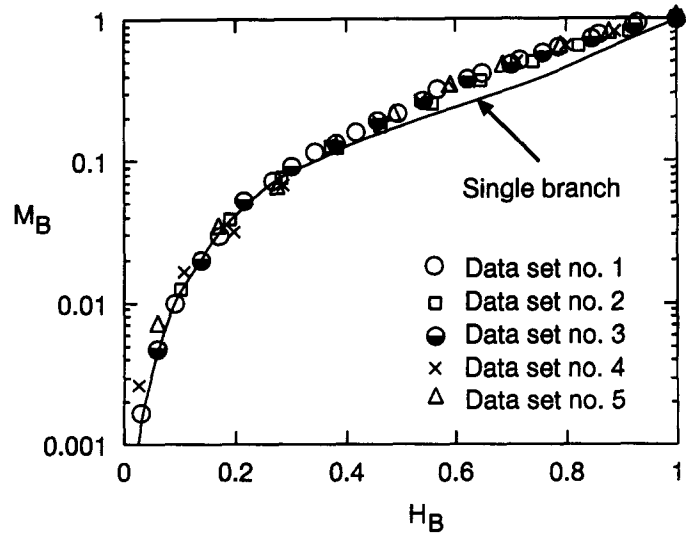

Figure 10. Values of M_B for data set nos 1–5.

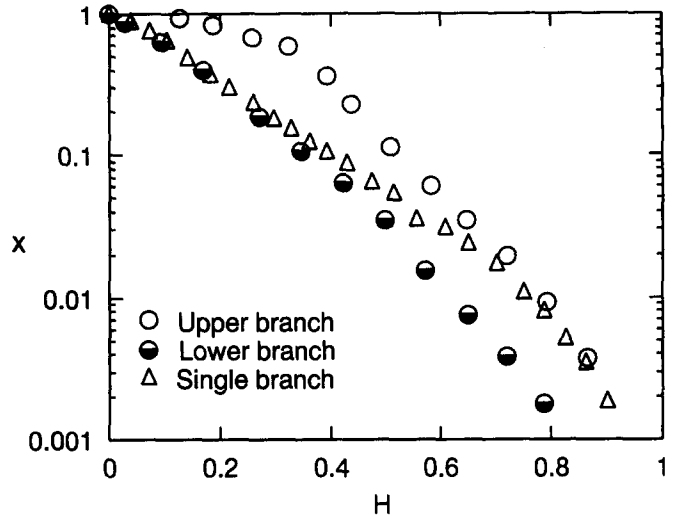

Figure 11. Discharge quality for data set no. 1.

It must be pointed out that for any value of L/d, the results for x and M at both branches should approach the single-branch results at sufficiently low values of ΔP or high values of R. As pointed out earlier in section 2.1, the two branches will behave essentially as two independent single branches if the onset of liquid entrainment at the upper branch corresponds to a higher interface level than that for the onset of gas entrainment at the lower branch. However, for the results in figures 9 and 10 ($L/d = 1.5$), this would require a very low ΔP of approximately 0.1 kPa at $P_0 = 517$ kPa and $R = 1000\ (\text{kg}\cdot\text{m})^{-1/2}$. All the results in data set nos 1–26 correspond to sufficiently high values of ΔP for which the interface level at the onset of liquid entrainment at the upper branch is lower than the interface level at the onset of gas entrainment at the lower branch. Thus, these data sets correspond to the condition where there is mutual interaction between the upper and lower branches. The trends in figures 9 and 10 showing the collapse of data for various ΔP and R are typical of all data in set nos 1–26.

An effect that could not be absorbed by these normalized plots is that of L/d. Figures 11 and 12 show normalized plots of discharge quality and mass flow rate, respectively, for data set no. 1 corresponding to $L/d = 1.5$. Very significant differences can be seen between the results for the upper branch and those for the lower branch. The upper-branch results converge to those of a single branch at high H and the lower-branch results converge to those of a single branch at low H. The

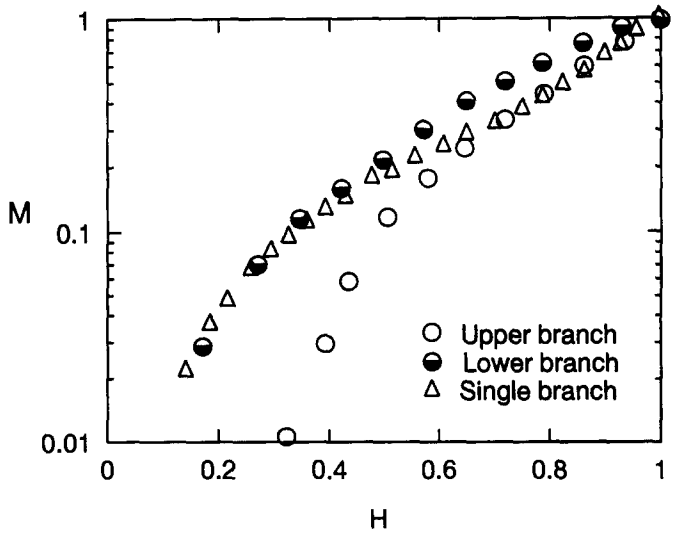

Figure 12. Normalized two-phase discharge for data set no. 1.

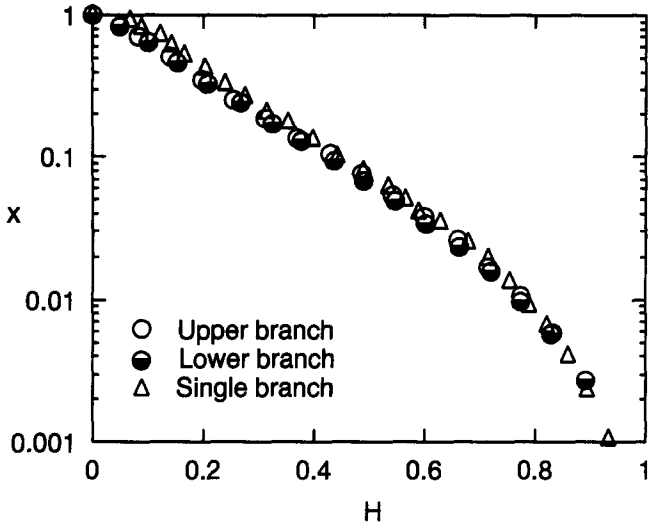

Figure 13. Discharge quality for data set no. 30.

difference between upper and lower branch results was found to decrease as L/d was increased while maintaining the same P_0, ΔP and R.

Figures 13 and 14 show that the results for both branches in data set no. 30 ($L/d = 8$) collapse on top of the single-branch data. This behaviour is typical of all data in set nos 27–32. All these data correspond to the condition where the onset of liquid entrainment at the upper branch occurs at a considerably higher interface level than that for the onset of gas entrainment at the lower branch and the two branches function as independent single branches.

It is understood that many industrial applications are considerably more complex than the experiment reported here, both in terms of the number of discharges and the interface being disturbed, as opposed to smooth. As mentioned earlier, the present experiment is meant to be a stepping stone, in terms of understanding the phenomena, toward the more complex cases as there was so little information on these cases. In the present case, with steady conditions and a smooth interface, accurate measurements are possible and qualitatively at least, some of the phenomena are expected to be the same as for the more complex cases. As regards the case of a disturbed interface, it is expected that at least in the present geometry, the behaviour of the mass flow rates of each phase with interface location, as described in the appendix, would be qualitatively the same

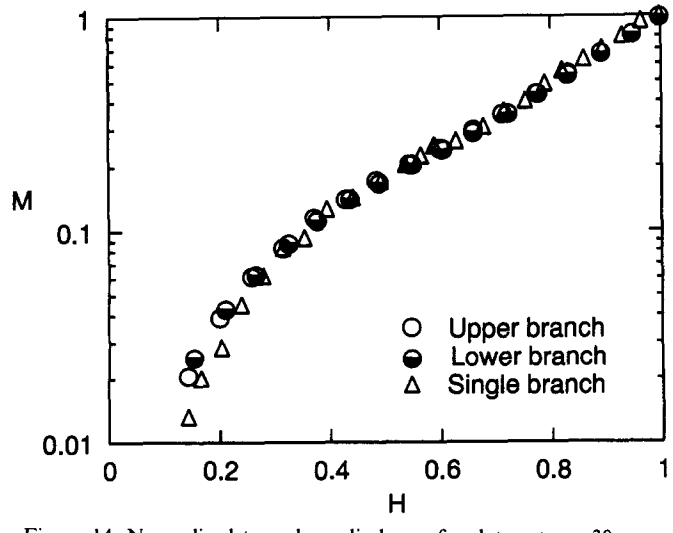

Figure 14. Normalized two-phase discharge for data set no. 30.

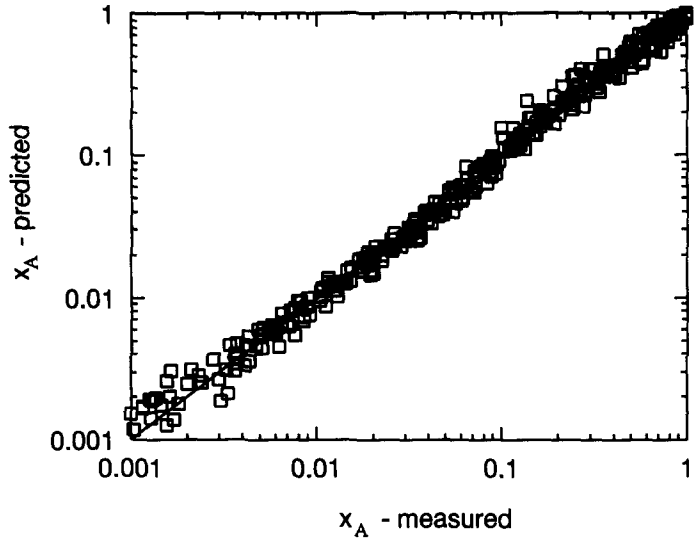

Figure 15. Predicted vs measured values of x_A.

as for a smooth interface; further experiments would be necessary to determine the quantitative behaviour.

3.3. Data correlation

An attempt was made to develop empirical relations for the prediction of x and M at both branches resulting in the following relations:

$$x_A = 0.2\exp[6H_A(1 - B_1H_A)/(1 - H_A)] + 0.8(1 - H_A^2)^{1.3}(B_2E)^{H_A}, \quad [16]$$

$$x_B = 0.2\exp[6H_B(1 - C_1H_B)/(1 - H_B)] + 0.8(1 - H_B^2)^{1.3}(C_2E)^{H_B}, \quad [17]$$

$$M_A = H_A^{[2 + B_3(1 - H_A^2)]}\exp[-1.84H_A^2(1 - H_A^2)^{1.318}] \quad [18]$$

and

$$M_B = H_B^2\exp[-1.84H_B^2(1 - H_B^2)^{C_3}], \quad [19]$$

where,

$$B_1 = 11.67 - 9.67\exp[-0.01(L/d)^3], \quad [20]$$

$$B_2 = 1 + 0.92\exp[-0.75(L/d)], \quad [21]$$

$$B_3 = 6.68\exp[-0.027(L/d)^4], \quad [22]$$

$$C_1 = 11.67 - 3.03\exp[-0.016(L/d)^3], \quad [23]$$

$$C_2 = 1 - 0.71\exp[-0.03(L/d)^4], \quad [24]$$

$$C_3 = 1.318 + 5.78\exp[-0.37(L/d)^2] \quad [25]$$

and

$$E = -0.0122 + 0.42/[1 + \sqrt{\rho_L/\rho_G}]. \quad [26]$$

At the limit $L/d = \infty$, the above relations converge to $B_1 = C_1 = 11.67$, $B_2 = C_2 = 1$, $B_3 = 0$ and $C_3 = 1.318$ and, consequently, [16]–[19] converge to the single-branch relations for x and M reported by Hassan (1995). Within the range $1.5 \leqslant L/d \leqslant 8$, the above empirical relations are in good agreement with the present data, as exemplified in figures 15 and 16. Quantitatively, the

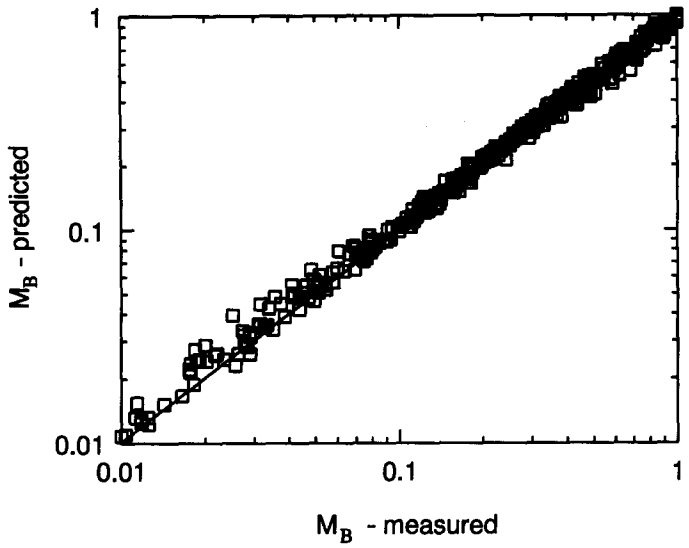

Figure 16. Predicted vs measured values of M_B.

discharge quality at the upper branch is predicted with a root-mean-square error of 16.7% over the range $0.001 \leqslant x_A \leqslant 1$, the discharge quality at the lower branch is predicted with a root-mean-square error of 18.1% over the range $0.001 \leqslant x_B \leqslant 1$, the normalized two-phase discharge at the upper branch is predicted with a root-mean-square error of 23.3% over the range $0.01 \leqslant M_A \leqslant 1$ and the normalized two-phase discharge at the lower branch is predicted with a root-mean-square error of 11.3% over the range $0.01 \leqslant M_B \leqslant 1$. All errors were found to decrease considerably when the segment of data corresponding to the smallest values of x and M was not considered.

4. CONCLUDING REMARKS

Experimental data are reported on the onsets of gas and liquid entrainment, mass flow rate and quality during two-phase discharge from a large reservoir through two small ($d = 6.235$ mm) side branches one above the other under stratified conditions. The experiments were conducted under the condition that the two discharges correspond to the same ΔP and the two lines connecting the test section to the separators have the same R. Thirty-two data sets were collected covering the ranges of $316 \leqslant P_0 \leqslant 517$ kPa, $40 \leqslant \Delta P \leqslant 235$ kPa, $1000 \leqslant R \leqslant 3000$ $(\text{kg}\cdot\text{m})^{-1/2}$, and $1.5 \leqslant L/d \leqslant 8$. The independent variables were varied in a systematic fashion in order to facilitate the study of the influence of each variable separately.

The present results indicate that $\dot{m}_{TP}$ and x for dual discharge can deviate significantly from the corresponding values for single discharge. This deviation increases with an increase in ΔP and/or a decrease in R or L/d. Influences of ΔP and R are shown to be largely absorbed (within the present test range) when normalized parameters are used in presenting the data. However, L/d remains as a parameter in these normalized plots. Within the present test range, deviations between dual discharge and single discharge are noted for $L/d = 1.5$, 2 and 3, while for $L/d = 8$, the results for dual discharge collapse on those of single disharge.

Empirical relations were developed for the prediction of the onsets of gas and liquid entrainment, the two-phase mass flow rate and quality at both branches using normalized parameters. These relations represent the data with a high degree of correlation; being empirical, however, the relations should be used only within the range of conditions under which the data were gathered.

Acknowledgements—This research was carried out as a collaboration between the University of Manitoba and the Whiteshell Laboratories of AECL Research. The financial assistance provided by the Natural Sciences and Engineering Research Council of Canada and the CANDU Owners Group (COG) is gratefully acknowledged.

REFERENCES

Armstrong, K. F., Parrott, S. D., Sims, G. E., Soliman, H. M. & Krishnan, V. S. 1992 Theoretical and experimental study of the onset of liquid entrainment during dual discharge from large reservoirs. *Int. J. Multiphase Flow* **18,** 217–227.

Hassan, I. G. 1995 Single, dual and triple discharge from a large, stratified, two-phase region through small branches. Ph.D. thesis, University of Manitoba.

Hassan, I. G., Soliman, H. M., Sims, G. E. & Kowalski, J. E. 1994 Two-phase flow from a large reservoir through a small side orifice. *Experimental and Computational Aspects of Validation of Multiphase Flow CFD Codes*, FED-Vol. 180, pp. 47–58, ASME FED Summer Meeting, Lake Tahoe, Nevada.

Henry, R. E. & Fauske, H. K. 1971 The two-phase critical heat flow of one-component mixtures in nozzles, orifices and short tubes. *J. Heat Transfer* **93**, 179–187.

Kline, S. J. & McClintock, F. A. 1953 Describing the uncertainties in single-sample experiments. *Mechanical Engineering J.* **75**, 3–8.

Micaelli, J. C. & Memponteil, A. 1989 Two-phase flow behaviour in a tee-junction: the CATHARE model. *Proc. 4th Int. Topical Meeting on Nuclear Reactor Thermal-hydraulics*, Vol. 2, pp. 1024–1030, Karlsruhe, Germany.

Moffat, R. J. 1988 Describing the uncertainties in experimental results. *Experimental Thermal and Fluid Science* **1,** 3–17.

Parrott, S. D., Soliman, H. M., Sims, G. E. & Krishnan, V. S. 1991 Experiments on the onset of gas pull-through during dual discharge from a reservoir. *Int. J. Multiphase Flow* **17,** 119–129.

Schrock, V. E., Revankar, S. T., Mannheimer, R., Wang, C. H. & Jia, D. 1986 Steam-water critical flow through small pipes from stratified upstream regions. *Proc. 8th Int. Heat Transfer Conf.*, pp. 2307–2311, San Francisco, CA.

Smoglie, C. & Reimann, J. 1986 Two-phase flow through small branches in a horizontal pipe with stratified flow. *Int. J. Multiphase Flow* **12,** 609–625.

Whalley, P. B. 1987 *Boiling, Condensation and Gas–Liquid Flow*, pp. 68–77. Oxford University Press, Oxford.

Yonomoto, T. & Tasaka, K. 1988 New theoretical model for two-phase flow discharged from stratified two-phase region through small break. *J. Nuclear Science and Technology* **25,** 441–455.

Yonomoto, T. & Tasaka, K. 1991 Liquid and gas entrainment to a small break hole from a stratified two-phase region. *Int. J. Multiphase Flow* **17,** 745–765.

Zuber, N. 1980 Problems in modeling of small break LOCA. Nuclear Regulatory Commission Report NUREG-0724.

APPENDIX

Flow Phenomena

This appendix describes the flow phenomena encountered in this experiment, and is meant to be self-contained. The flow phenomena are described in terms of the mass flow rate of each phase and the appearance of the interface, these as a function of h^*, where h^* is the distance of the flat part of the interface above some datum located arbitrarily well below the lower branch; this definition of h^* is shown in figure A1(c). The terms "simple case" and "complex case" are used and mean those situations where $h^*_{\mathrm{BLE.A}} > h^*_{\mathrm{BGE.B}}$ and $h^*_{\mathrm{BLE.A}} < h^*_{\mathrm{BGE.B}}$, respectively, where $h^*_{\mathrm{BLE.A}}$ and $h^*_{\mathrm{BGE.B}}$ are the values of h^* at the beginning of liquid entrainment at the upper branch and the beginning of gas entrainment at the lower branch, respectively. The interface shape is sketched approximately to scale for $L/d = 8$ (simple case) and $L/d = 2$ (complex case), both with large ΔP and small R.

The simple case ($h^*_{\mathrm{BLE.A}} > h^*_{\mathrm{BGE.B}}$)

$h^* \geqslant h^*_{\mathrm{BGE.A}}$ *(see region 1 in figure A2).* Let us begin with an interface level well above the upper branch. Both branches will be flowing liquid only, the flow rates of which will be essentially the same, i.e. $\dot{m}_{\mathrm{L.A}} = \dot{m}_{\mathrm{L.B}}$ as shown in figure A2 and the interface will be flat as shown in figure A1(a). As h^* is lowered and approaches $h^*_{\mathrm{BGE.A}}$ a "dimple" begins to form in the interface (figure A1(b)).

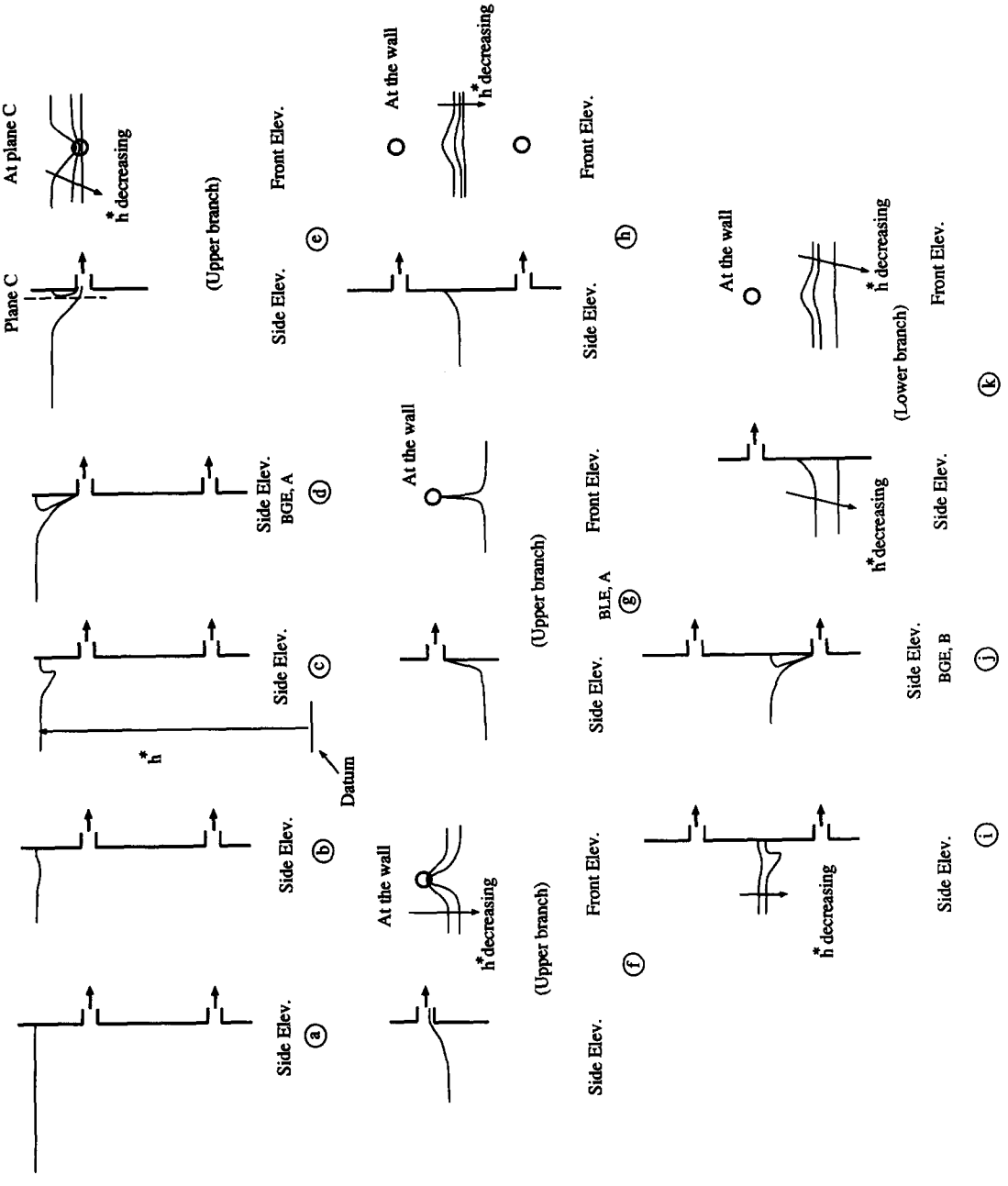

Figure A1—*see caption overleaf*

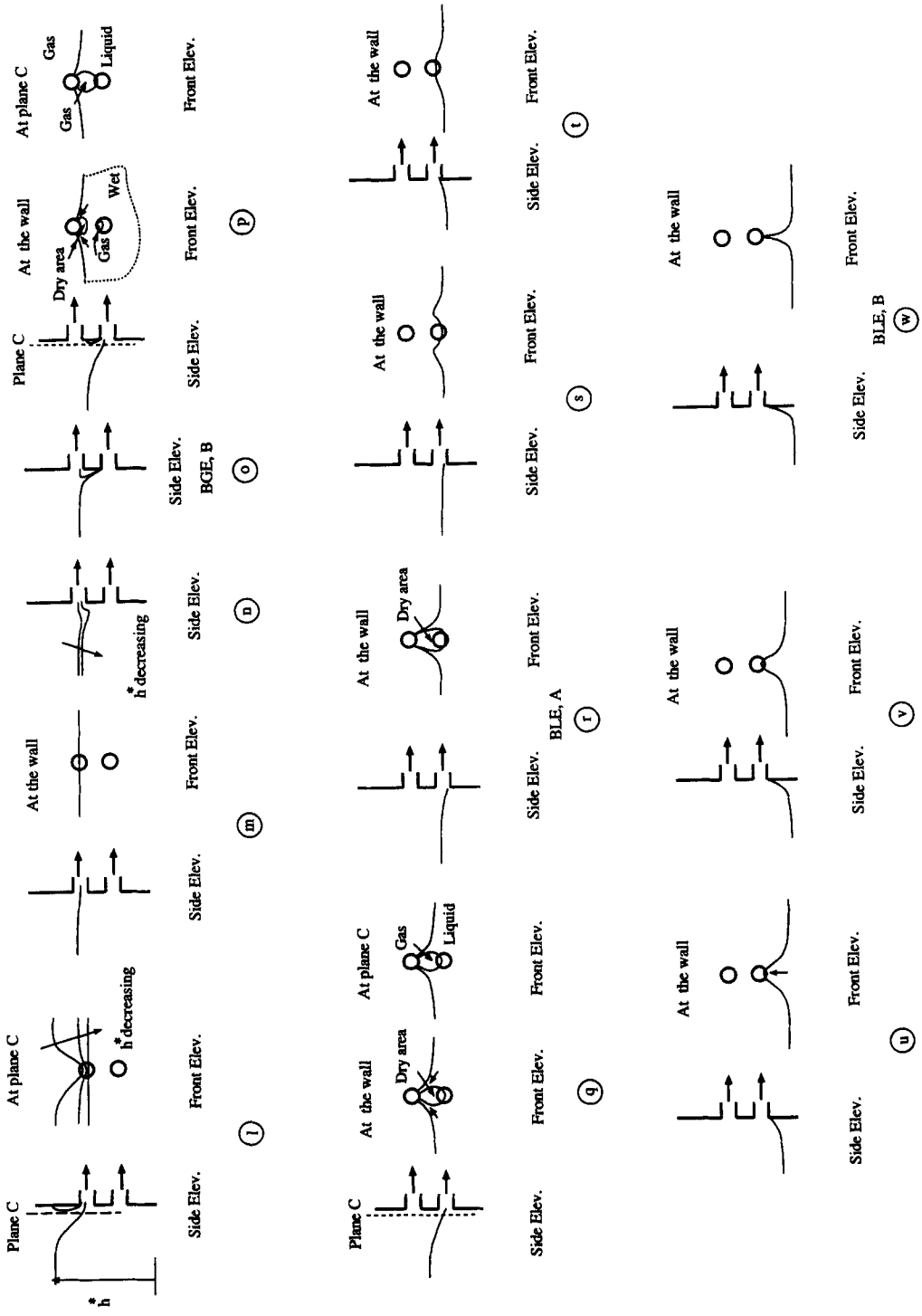

Figure A1. Sketches of the interface shape.

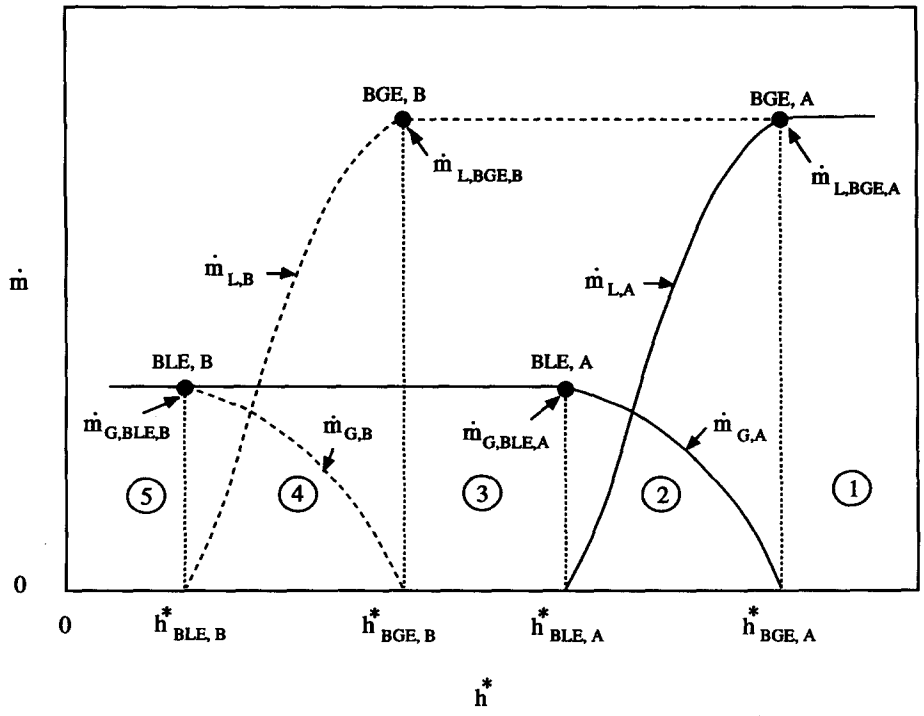

Figure A2. Qualitative mass flow rates for the simple case ($h^*_{BLE,A} > h^*_{BGE,B}$).

This depression becomes more pronounced (figure A1(c)) and cone-like until the bottom of the cone suddenly extends to the upper branch; this is the beginning of gas entrainment at the upper branch BGE,A (figure A1(d)); the corresponding h^* is $h^*_{BGE,A}$ and the flow rates are $\dot{m}_{L,A} = \dot{m}_{L,B} = \dot{m}_{L,BGE,A}$. In figure A.1, sketches marked "side elevation" are taken along a vertical plane through the centrelines of the two branches.

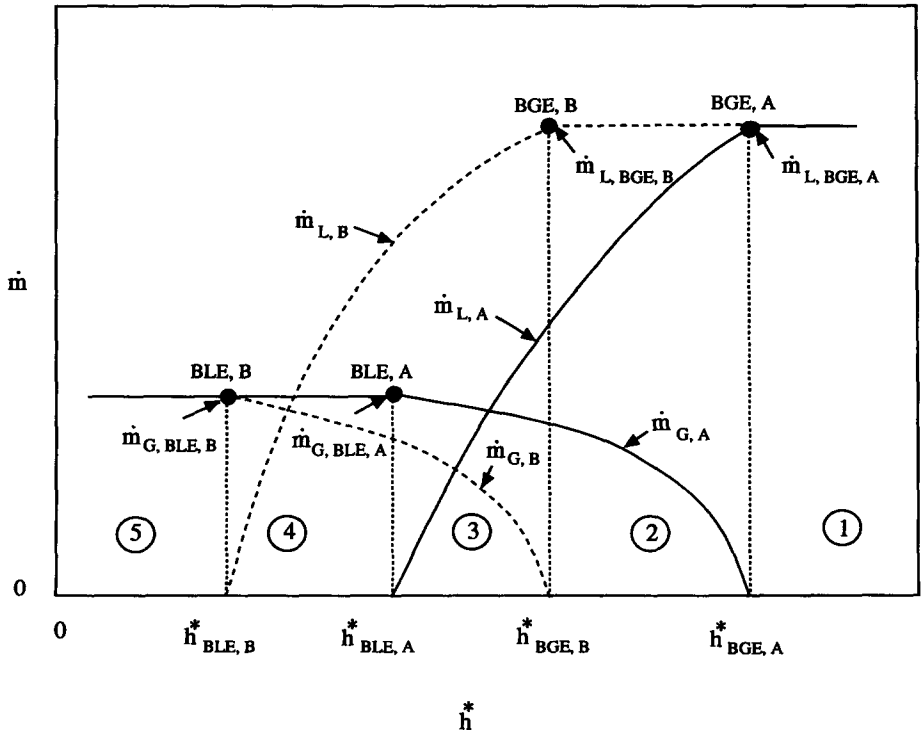

Figure A3. Qualitative mass flow rates for the complex case ($h^*_{BLE,A} < h^*_{BGE,B}$).

$h^*_{BGE,A} > h^* \geqslant h^*_{BLE,A}$ *(see region 2 in figure A.2).* In this range the lower branch continues to flow only liquid at the rate $\dot{m}_{L,B} = \dot{m}_{L,BGE,A}$ At the upper branch $\dot{m}_{L,A}$ decreases and $\dot{m}_{G,A}$ increases as h^* decreases. The interface shape is shown through figure A1(e) and (f) until at (g) liquid is no longer entrained at the upper branch, i.e. $\dot{m}_{L,A} = 0$ and $h^* = h^*_{BLE,A}$ while the corresponding gas flow rate at the upper branch is $\dot{m}_{G,BLE,A}$.

$h^*_{BLE,A} > h^* \geqslant h^*_{BGE,B}$ *(see region 3 in figure A2).* As h^* is reduced below $h^*_{BLE,A}$, the upper branch flows only gas at the rate of $\dot{m}_{G,A} = \dot{m}_{G,BLE,A}$. The lower branch continues to flow only liquid at the rate of $\dot{m}_{L,B} = \dot{m}_{L,BGE,A}$. With decreasing h^*, the interface is depicted in figure A1(h) and (i). In (i) a dimple in the interface has begun to form, becomes more pronounced and cone-like and finally the tip of the cone extends to the lower branch, as depicted in figure A.1(j). This is the beginning of gas entrainment at the lower branch; the h^* is $h^*_{BGE,B}$ and the various flow rates are $\dot{m}_{G,A} = \dot{m}_{G,BLE,A}$, $\dot{m}_{L,A} = 0$, $\dot{m}_{G,B} = 0$ (onset) and $\dot{m}_{L,B} = \dot{m}_{L,BGE,B}$ $(= \dot{m}_{L,BGE,A})$.

$h^*_{BGE,B} > h^* \geqslant h^*_{BLE,B}$ *(see region 4 in figure A2).* In this range, the interface shape would be as depicted in figure A1(e), (f) and (g), excepting, of course, at the lower branch. The "onset" or "beginning" of liquid entrainment is at $h^*_{BLE,B}$ at which the various flow rates are $\dot{m}_{G,A} = \dot{m}_{G,BLE,A}$, $\dot{m}_{L,A} = 0$, $\dot{m}_{G,B} = \dot{m}_{G,BLE,B}$ $(= \dot{m}_{G,BLE,A})$, $\dot{m}_{L,B} = 0$ (onset).

$h^* < h^*_{BLE,B}$ *(see region 5 in figure A2).* In this range, the interface shape would be as depicted in figure A.1(k); when h^* is sufficiently small the interface is flat. The flow rates in this region are $\dot{m}_{G,A} = \dot{m}_{G,B} = \dot{m}_{G,BLE,A} = \dot{m}_{G,BLE,B}$ and $\dot{m}_{L,A} = \dot{m}_{L,B} = 0$.

The complex case $(h^*_{BLE,A} < h^*_{BGE,B})$

$h^* \geqslant h^*_{BGE,A}$ *(see region 1 in figure A3).* The description is the same as for the simple case, including references to the sketches (except for the distance between the branches and $h^*_{BGE,A}$ being larger in the present case).

$h^*_{BGE,A} > h^* \geqslant h^*_{BGE,B}$ *(see region 2 in figure A3).* In this range the lower branch continues to flow only liquid at the rate $\dot{m}_{L,B} = \dot{m}_{L,BGE,A}$ while at the upper branch $\dot{m}_{L,A}$ decreases (from a value of $\dot{m}_{L,BGE,A}$) and $\dot{m}_{G,A}$ increases as h^* decreases. The interface shape is shown in figure A1(1), (m) and (n) with a cone being formed at the lower values of h^* until at (o) the tip of the cone extends to the lower branch when $h^* = h^*_{BGE,B}$.

$h^*_{BGE,B} > h^* \geqslant h^*_{BLE,A}$ *(see region 3 of figure A3).* In this region both branches are flowing a two-phase mixture. As h^* is lowered, the liquid flow rate $\dot{m}_{L,A}$ and gas flow rate $\dot{m}_{G,A}$ at the upper branch continue to decrease and increase, respectively. Similarly, for the lower branch $\dot{m}_{L,B}$ decreases while $\dot{m}_{G,B}$ increases. Liquid is fed to the upper branch in two streams from the sides of the branch. A "trough" of gas feeds gas to the lower branch. The interface shapes are sketched in figure A1(p) and (q). The streams feeding liquid to the upper branch become thinner as h^* is decreased until the flow of liquid into the upper branch ceases $(\dot{m}_{L,A} = 0)$; this is at $h^*_{BLE,A}$ and the interface is sketched in figure A1(r); at this point $\dot{m}_{G,A} = \dot{m}_{G,BLE,A}$, the maximum $\dot{m}_{G,A}$.

$h^*_{BLE,A} > h^* \geqslant h^*_{BLE,B}$ *(see region 4 in figure A3).* Here the upper branch is flowing gas only at $\dot{m}_{G,A} = \dot{m}_{G,BLE,A}$ while the lower branch is flowing a two-phase mixture. The interface shapes are shown in figure A1(s)–(v) as h^* is decreased. The liquid being sucked up the wall as in (v) diminishes to zero as h^* is decreased to $h^*_{BLE,B}$; this is shown in figure A1(w) at which point $\dot{m}_{L,B} = 0$ and $\dot{m}_{G,B} = \dot{m}_{G,BLE,B}$ $(= \dot{m}_{G,BLE,A})$, the maximum gas flow rate in the lower branch.

$h^* < h^*_{BLE,B}$ *(see region 5 in figure A3).* Here both branches are flowing gas only and the various flow rates are: $\dot{m}_{L,A} = \dot{m}_{L,B} = 0$ and $\dot{m}_{G,A} = \dot{m}_{G,B} = \dot{m}_{BLE,A} = \dot{m}_{BLE,B}$. The interface shapes are essentially as shown in figure A1(k).